Mathematical Modelling and Control

https://www.aimspress.com/journal/mmc

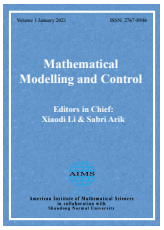

MMC, 4(4): 374–389.
DOI: 10.3934/mmc.2024030
Received: 25 August 2023
Revised: 01 April 2024
Accepted: 28 June 2024
Published: 13 November 2024

Research article

A frequency domain-based loop shaping procedure for the parameter estimation of the fractional-order tilt integral derivative controller

Biresh Kumar Dakua* **and Bibhuti Bhusan Pati**

Department of Electrical Engineering, Veer Surendra Sai University of Technology, Odisha 768018, India

* **Correspondence:** Email: bireshdakua@gmail.com.

Abstract: This paper demonstrates a frequency domain-based loop shaping method for the parameter estimation of a fractional order tilt integral derivative (FOTID) controller for the interval integer and fractional order time-delay systems. Along with the five nonlinear constraints usually considered for the design of the fractional order proportional integral derivative (FOPID) controller, a more flat phase concept signifying an enhanced robustness of the system towards gain variations is adopted as the sixth constraint for the tuning of a six variable tunable FOTID controller. The optimization toolbox fmincon in MATLAB is utilized for the solution process of the above constraint minimization problem. A certain class of fractional order plus time delay process is considered for the implementation and validation of the above procedure. The robustness of the FOTID controller optimized by the proposed method is tested against variations of the system parameters. By considering different numerical examples, the technical superiority of the FOTID controller over the FOPID controller is demonstrated through suitable comparisons in this current work.

Keywords: fractional order system; fractional order controller; TID controller; FOTID controller; parameter estimation; loop shaping method; robustness analysis

1. Introduction

In the feedback control system, controllers are used to compensate for the deficiencies inherited in the process dynamics. The use of integer order controllers such as the proportional-integral (PI) or the proportional-integral-derivative (PID) is more frequent in process industries. Here, the proportional gain constant (K_P) magnifies the signal amplitude, the integral gain constant (K_I) nullifies the error, and the derivative gain constant (K_D) minimizes the overshoot by presenting suitable damping to the system [1]. Due to the evolution of the computational methods, a shift towards fractional calculus is noticed in the last decades [2]. It is well proven that the dynamics of complex physical systems can better be captured in terms of fractional calculus [3, 4]. The non-integral (fractional) order systems and controllers are widely studied, and multiple tools for the analysis of non-integer order systems are proposed in [5, 6]. A fractional order controller was proposed by [7], where the PID was modified with a fractional-integral $\left(\frac{K_I}{S^\lambda}\right)$ and a fractional-derivative term ($K_D s^\mu$). Here, λ, μ are the fractional exponents ranging (0, 2), which provided an improved system performance in comparison with the conventional PID [8, 9]. A unique tilt integral derivative controller (TID) was presented in [10], where, in accordance with the PID, the proportional gain constant (K_T) was multiplied with a tilt exponent $\left(S^{-1/n}\right)$. The tilt factor usually introduces damping to the system, approximates the optimal transfer function, provides a simpler tuning approach, and produces a robust system performance.

Similar to every controller, a TID controller can also be tuned in both the time and frequency domain approaches. While the frequency domain method depends on the phase margin (PM), and the gain margin (GM) based a loop shaping procedure, the time domain method mostly relies on the nullification of error-based objective functions. On

one hand, due to the availability of different optimization strategies, the time domain tuning is more frequent [11]; on the other hand, because of mathematical complicacy, the frequency domain tuning is rare. As mentioned below, very few articles discuss the analytical evaluation of TID. A PM, GM-based frequency domain TID tuning method for a fractional order time delay processes is presented in [12]. A similar frequency domain loop shaping strategy for TID controllers with first-order as well as higher-order systems consideing time delays are mentioned in [13]. An analytical procedure for the parameter estimation of the TID controller for non-integer order interval systems is provided in [14]. An linear matrix inequality-based TID tuning strategy for integer and non-integer order processes is demonstrated in [15]. The time domain-based tuning of TID and its corresponding applications in power system problems such as frequency regulation and voltage stability are mentioned in many articles using various optimization algorithms to solve for different cost functions. The use of the equilibrium optimizer with an integral of square error (ISE) as a cost function for the frequency control of integrated power system is presented in [16].

The nonlinear optimization toolbox fmincon() to minimize integral time absolute error (ITAE) was used for the frequency control of a power system in [17]. The wild horse optimizer using TID and fuzzy fractional order proportional integral was tuned by minimizing the ISE for the frequency control of a power system as shown in [18]. The arithmetic optimization algorithm in association with the particle swarm optimization (PSO), the teaching learning-based optimization, and the artificial bee colony for the frequency control of restructured power system are demonstrated in [19]. The Runge Kutta optimizer has been used for the stability of the power system by suppressing the integral time square error [20]. The differential evolution (DE) has been used for the frequency regulation of power systems by considering ITAE as an objective function [21]. The adaptive DE with minimization of the ITAE has been used for the frequency control by tuning of the TID with a filter [22]. In [23], the genetic algorithm (GA), the firefly algorithm, the PSO, and the DE were used for the frequency regulation of multi-area power systems using a TID controller, thereby having the ITAE as a cost function. The use of a combined dragonfly algorithm and pattern search algorithm for frequency regulation in microgrids is mentioned in [24] by using the TID with ITAE. An imperialistic competitive algorithm that minimized various error-based cost functions for the tuning of the tilt integrator differentiator with filter controller towards the microgrid frequency regulation is presented in [25]. The use of the artificial hummingbird algorithm for the tuning of fuzzy-TID by considering ISE is mentioned in [26] for the control of multi-area energy systems. Likewise, the use of the sailfish optimizer to solve microgrid frequency control problems using the fuzzy-TID considering ISE is shown in [27]. Similarly, in [28], the application of the fuzzy-TID for the frequency control of microgrid systems by considering ITAE as a cost function is presented.

The application of the TID to many other control systems is also reported in the literature. A fitness distance balance-based Runge Kutta optimizer was used for the parameter debugging of the TID controller by considering various error-based cost functions and was used for the voltage control of a buck converter system [29]. Moreover, the use of the GA while considering certain objective functions for the tuning of TID to address the speed control of a permanent magnet synchronous motor is mentioned in [30]. The use of the flower pollination algorithm for the parameter estimation of the TID by minimizing different cost functions towards the regulation of electric machines is demonstrated in [31]. A bird swarm algorithm for the optimal tuning of TID controllers in the automatic generation control problem of the power system is mentioned in [32]. Furthermore, an extension of these above concepts towards multi-input multi-output systems is presented in [33]. Similarly, this article also uses PSO to tune the TID controller.

A modified TID controller, that has a fractional-integral $\left(\frac{K_I}{S^\lambda}\right)$ and a fractional-derivative term ($K_D s^\mu$) along with the tilt component $\left(\frac{K_T}{s^{1/n}}\right)$ is termed a fractional order tilt integral derivative (FOTID) controller. Although it is structurally analogous to that of the fractional order proportional integral derivative (FOPID) controller, it inherits the tilted behavior of the TID controllers. The tilt structure and the fractional calculus enable the FOTID controllers to provide an improved, robust control of the physical dynamical systems. This advantage encourages the researchers to use

optimized FOTID controllers for their respective problem statements. Similar procedures can be adopted for the parameter estimation of the FOTID controller by minimizing suitable objective functions. The use of the pathfinder algorithm to tune the FOTID by suppressing ITAE for the voltage control of the power system is presented in [34]. A salp swarm algorithm that tuned the FOTID by minimizing ITAE is proposed in [35] for the frequency control of the power system. Similarly, in [36], the Harris hawk optimizer that considered the ISE as a cost function was used for the parameter estimation of the FOTID and the frequency regulation of a power system. A combined PSO and GA were used to tune the FOTID controller by adopting ITAE for the control of a photovoltaic system [37].

The use of the gray wolf optimization and the whale optimization algorithm to tune the parameter of the FOTID by suppressing different error functions for the speed regulation of the direct current motor is demonstrated in [38]. The artificial hummingbird algorithm tuned the FOTID with a fractional filter and considered different objective functions for the frequency regulation of a power system [39]. In [40], a dual-stage FOTID-PD controller was proposed and tuned by the salp swarm algorithm and considered ITAE for the frequency control in the power system. A GA-optimized fuzzy-FOTID controller was used for the process control problem by considering various cost functions [41]. A Honey Badger algorithm that tuned the FOTID controller for the automatic generation control of the electric power system [42]. An internal model control scheme for the tuning of the FOTID and the control of unstable processes including time lags is demonstrated in [43]. Furthermore, similar to the proportional-integral plus proportional-derivative controller, a unique tilt integral plus tilt derivative controller was proposed in [44], where the controller is tuned by the water cycle algorithm by considering different error functions for the frequency control of the energy system.

From the literature study, it is observed that the parameter estimation of the TID and the FOTID has mostly been performed by using different optimization techniques in the time domain. The nullification of error-based objective functions is the modus operandi in all of the aforementioned stochastic procedures. Even if this process of tuning the controllers is easy, it does not provide any clear insight regarding the procedure. During every execution, the optimization algorithms produce different results and the prediction of the lower and upper bounds of the variables is also a trial-and-error procedure. A very scant literature described the frequency domain-based parameter tuning of the TID; it was because of the difficulties of six optimizable parameters. It should be noted that, while the TID requires at least four equations, the FOTID needs six simultaneous equations in the frequency domain based loop shaping process to produce suitable results. A detailed description of the FOTID tuning using the loop shaping strategy was not mentioned in any article.

This article presents a deterministic design strategy for the parameter estimation of the six-parameter tunable FOTID controller. The frequency domain-based loop shaping procedure is discussed here, which is comprised of six equations to tune the FOTID controller. As the loop shaping method which considers the GM, PM, flat phase, noise, and disturbance rejection constraints for five parameters tunable FOPID controller is already present in literature [8, 45], this article adds a more-flat phase concept [46] as the sixth constraint for the tuning process of FOTID controllers.

Some of the major contributions of this research article are discussed below:

- A loop shaping-based parameter estimation method for the FOTID controller achieves the desired system performance.
- A more-flat phase concept is added as the sixth constraint for an analytical evaluation of FOTID controller parameters.
- Tuning of FOTID for fractional and integral order interval systems is demonstrated through suitable examples.

The orientation of this research article is as per the following: Section 2 details the information about the control system under consideration; Section 3 presents the mathematical modeling of the FOTID controller; Section 4 provides the loop-shaping strategy to tune the FOTID controllers; Section 5 demonstrates the advantages of the proposed procedure through suitable numerical examples; and finally, Section 6 presents the concluding words and a glimpse of future work.

2. System under observation

Consider a feedback control system which consists of a non-integer (fractional) order plant, as shown in Figure 1.

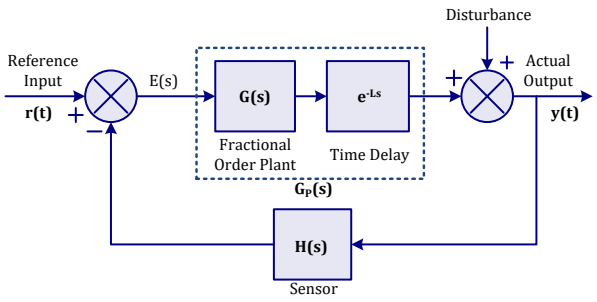

Figure 1. A non-integer order feedback control loop.

The dynamics of the fractional order plus time delay process model is presented as follows [47]:

$$G_P(s) = \frac{K'}{\tau s^{\alpha} + 1} e^{-Ls} = \frac{K}{s^{\alpha} + a} e^{-Ls}. \tag{2.1}$$

Where,

$$K = \frac{K'}{\tau} \text{ and } a = \frac{1}{\tau}.$$

Here, K is the system gain, a is the integer order system pole, α is the fractional exponent, and L is the time delay of the above system. This could be converted to an integer order system (i.e., first-order plus time delay system simply by assigning $\alpha = 1$). A frequency domain-based analysis of the above system can be performed by replacing the operator $s \Rightarrow j\omega$, thereby splitting the fractional function $G_P(j\omega)$ into its corresponding magnitude and phase angle form, as detailed below:

$$G_P(j\omega) = \frac{K}{(j\omega)^{\alpha} + a} e^{-j\omega L}.$$

Now, according to De-Moivre's theorem,

$$(j\omega)^n = \omega^n \left(cos\frac{n\pi}{2} + jsin\frac{n\pi}{2} \right). \tag{2.2}$$

Therefore, the above equation becomes the following:

$$G_P(j\omega) = \frac{K}{\omega^{\alpha}(cos\frac{\alpha\pi}{2} + jsin\frac{\alpha\pi}{2}) + a} e^{-j\omega L},$$

$$\Rightarrow G_P(j\omega) = \frac{K}{(a + \omega^{\alpha} cos\frac{\alpha\pi}{2}) + j(\omega^{\alpha} sin\frac{\alpha\pi}{2})} e^{-j\omega L}.$$

Hence, the above system can be separated in terms of its magnitude and phase as follows:

$$|G_P(j\omega)| = \frac{K}{\sqrt{(a + \omega^{\alpha} cos\frac{\alpha\pi}{2})^2 + (\omega^{\alpha} sin\frac{\alpha\pi}{2})^2}}, \tag{2.3}$$

$$\angle G_P(j\omega) = -\tan^{-1}\left(\frac{\omega^{\alpha} sin\frac{\alpha\pi}{2}}{a + \omega^{\alpha} cos\frac{\alpha\pi}{2}} \right) - \omega L. \tag{2.4}$$

Now, depending on the parameters, this paper analyses the dynamics of the system and implements an FOTID controller to achieve the desired performance.

3. The FOTID controller

An FOTID controller which has a fractional integral and derivative component along with a tilt factor is considered for the performance enhancement of the above fractional system, as shown in Figure 2.

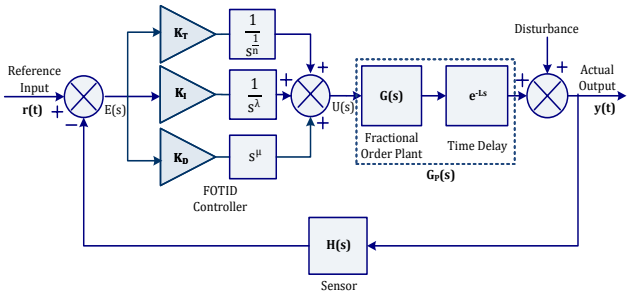

Figure 2. A non-integral feedback control system with FOTID controller.

The transfer function of the non-integer order TID controller is mathematically represented as follows [10, 34]:

$$G_C(s) = \frac{K_T}{s^{\frac{1}{n}}} + \frac{K_I}{s^{\lambda}} + K_D s^{\mu}, \quad \lambda, \mu, n > 0. \tag{3.1}$$

Here, K_T, K_I, and K_D are the proportional, integral, and differential coefficients respectively, while the fractional exponents $\lambda, \mu \in (0, 2)$, the tilt factor $n \in (2, 3)$. An appropriate parametric value of K_T, K_I, K_D, λ, μ, and n can produce the desirable closed-loop performance. The magnitude and the phase angle of the applied FOTID controller in a steady state using De-Moivre's theorem are evaluated as follows:

$$G_C(s) = K_T s^{\frac{-1}{n}} + K_I s^{-\lambda} + K_D s^{\mu}.$$

Assuming $\frac{1}{n} = \vartheta$, the above equation in a steady state is as follows:

$$\begin{aligned} G_C(j\omega) =& K_T(j\omega)^{-\vartheta} + K_I(j\omega)^{-\lambda} + K_D(j\omega)^{\mu}, \\ \Rightarrow G_C(j\omega) =& K_T\omega^{-\vartheta}\left(cos\frac{\vartheta\pi}{2} - jsin\frac{\vartheta\pi}{2}\right) \\ &+ K_I\omega^{-\lambda}\left(cos\frac{\lambda\pi}{2} - jsin\frac{\lambda\pi}{2}\right) \\ &+ K_D\omega^{\mu}\left(cos\frac{\mu\pi}{2} + jsin\frac{\mu\pi}{2}\right). \end{aligned}$$

Therefore, we have the following:

$$|G_C(j\omega)| = \sqrt{M^2 + N^2}, \tag{3.2}$$

$$\angle G_C(j\omega) = \tan^{-1}\left(\frac{N}{M}\right). \tag{3.3}$$

Here,

$$\begin{aligned} M &= K_D\omega^{\mu}cos\frac{\mu\pi}{2} + \frac{K_T}{\omega^{\vartheta}}cos\frac{\vartheta\pi}{2} + \frac{K_I}{\omega^{\lambda}}cos\frac{\lambda\pi}{2}, \\ N &= K_D\omega^{\mu}\sin\frac{\mu\pi}{2} - \frac{K_T}{\omega^{\vartheta}}\sin\frac{\vartheta\pi}{2} - \frac{K_I}{\omega^{\lambda}}\sin\frac{\lambda\pi}{2}. \end{aligned}$$

Furthermore, the TID controller is a special case of the FOTID controller having $\lambda = 1$ and $\mu = 1$. Therefore its corresponding transfer function is as follows:

$$G_{C-TID}(s) = \frac{K_T}{s^{\frac{1}{n}}} + \frac{K_I}{s} + K_D s. \tag{3.4}$$

Now, a unique strategy for the frequency domain-based parameter debugging of the FOTID controller is presented in the next section.

4. Frequency domain-based tuning strategy for FOTID controller

The major highlight of this research article is the proposal of a frequency domain-based parameter estimation strategy for the FOTID controller. A FOTID controller that is comprised of six unknown parameters (i.e., K_T, K_I, K_D, λ, μ, and n) requires at least six equations for an analytical evaluation. Therefore, along with the five loop shaping criteria used for the evaluation of the FOPID controllers (see [8, 46]), this paper applies a "more-flat phase" concept, as an additional requirement for the performance enhancement of the system with the FOTID controllers [45]

$$\frac{d^2\phi}{d^2\omega} = 0.$$

Here, ϕ is the phase angle of the corresponding system.

In the control system analysis, the phase margin is an important parameter that signifies the amount of phase angle by which a system can be increased or decreased without losing its stability. A higher phase margin is usually a measure of better stability and robustness. The "flat phase" response indicates that the phase angle shift of the system remains almost constant over different frequencies. The iso-damping property forces the phase angle plot to be flat and remain almost constant within the interval around the gain cross-over frequency [8].

Since the derivative indicates the rate of change of a variable, the flat phase $\left(\frac{d\phi}{d\omega} = 0\right)$ (i.e., no phase change) signifies the robustness of any system. Hence, the system becomes more consistent towards the gain variations. Likewise, as the second derivative measures the rate of change of the first derivative; therefore, can provide an enhanced robustness to the systems

$$\frac{d^2\phi}{d^2\omega} = 0.$$

The enhanced iso-damping property forces the phase angle plot to be flatter at ω_C (more-flat phase), thus displaying an even more consistent behavior within the interval around ω_C. It signifies that the system becomes more insensitive to open-loop gain variations [45].

4.1. FOTID tuning method

The tuning process of the FOTID is based on the solution of a set of constraint equations in the frequency domain. The parameters of the controller that satisfies the close loop requirements are the problem of a numerical optimization with constraints. The frequency-domain tuning scheme for the controller can be expressed as the following system requirements. The open-loop transfer function $T(s)$ that satisfies the plant $G_P(s)$, the feedback $H(s) = 1$ and the controller $G_C(s)$, should also satisfy the following frequency-domain design specifications.

4.1.1. Phase margin specification

The phase margin is related to the damping of the system and limits the close loop system overshoot [8]. Hence, it is regarded as an index for the performance of the system.

Therefore, the following condition must be satisfied:

$$Arg\left[T\left(j\omega_C\right)\right] = -\pi + \phi_m,$$

i.e.,

$$Arg\left[G_P(j\omega_C)G_C(j\omega_C)\right] = -\pi + \phi_m. \tag{4.1}$$

Here, ω_C is the gain cross-over frequency and ϕ_m is the desired phase margin.

4.1.2. Gain cross-over frequency specification

This ensures a specific settling time, hence an important measure of the stability of the system [8], i.e.,

$$\left|T\left(j\omega_C\right)\right|_{dB} = \left|G_P\left(j\omega_C\right)G_C\left(j\omega_C\right)\right|_{dB} = 0dB,$$

i.e.,

$$\left|T(j\omega_C)\right| = \left|G_P(j\omega_C)G_C(j\omega_C)\right| = 1. \tag{4.2}$$

4.1.3. Robustness to gain variation

The robustness of a system to gain variation desires the phase derivative w.r.t. the frequency to be zero [8]. This gives the following:

$$\frac{d}{d\omega}\left(Arg\left[T\left(j\omega\right)\right]\right)\Big|_{\omega=\omega_c} = 0,$$

i.e.,

$$\frac{d}{d\omega}\left(Arg\left[G_P(j\omega)G_C(j\omega)\right]\right)\Big|_{\omega=\omega_c} = 0. \tag{4.3}$$

4.1.4. Rejection of output disturbance

To ensure a good disturbance rejection property, the following condition for the sensitivity function $S(j\omega)$ has to be fulfilled [8]:

$$\left|S\left(j\omega\right)\right|_{dB} \leq B_D dB, \quad \forall\omega \leq \omega_s,$$

i.e.,

$$\left|\frac{1}{1 + G_P\left(j\omega\right)G_C\left(j\omega\right)}\right|_{dB}\Bigg|_{\omega=\omega_s} = B_D dB. \tag{4.4}$$

Here, B_D is the desired value of the sensitivity function for the cut-off frequency $\omega \leq \omega_s$ rad/sec.

4.1.5. Rejection of high-frequency noise

To attend to the robustness against high-frequency noise, the close loop frequency response $P(j\omega)$ (i.e., the complementary sensitivity function) has to satisfy the following low pass filtering requirement [8]:

$$\left|P\left(j\omega\right)\right|_{dB} \leq A_N dB, \quad \forall\omega \geq \omega_t,$$

i.e.,

$$\left|\frac{G_P\left(j\omega\right)G_C\left(j\omega\right)}{1 + G_P\left(j\omega\right)G_C\left(j\omega\right)}\right|_{dB}\Bigg|_{\omega=\omega_t} = A_N\ dB. \tag{4.5}$$

Here, $P(s)$ is the unit negative feedback closed-loop transfer function and A_N is the desired value of noise attenuation for the cut-off frequency $\omega \geq \omega_t$ rad/seconds.

4.1.6. Enhanced robustness to gain variation

A higher derivative can increase the iso-damping property of the system response and provide an improved robustness of the system towards the gain variation [45]

$$\frac{d^2}{d^2\omega}\left(Arg\left[T\left(j\omega\right)\right]\right)\Big|_{\omega=\omega_c} = 0,$$

i.e.,

$$\frac{d^2}{d^2\omega}\left(Arg\left[G_P(j\omega)G_C(j\omega)\right]\right)\Big|_{\omega=\omega_c} = 0. \tag{4.6}$$

4.2. FOTID tuning procedure

The parameter estimation of the FOTID using the above-mentioned loop shaping conditions is demonstrated as follows. Let us assume the following factors for simplicity in expressing the equations:

$$\begin{aligned}
A =& a + \omega^{\alpha}\cos\frac{\alpha\pi}{2}, \quad B = \omega^{\alpha}\sin\frac{\alpha\pi}{2},\\
C =& \alpha\omega^{\alpha-1}\cos\frac{\alpha\pi}{2}, \quad D = \alpha\omega^{\alpha-1}\sin\frac{\alpha\pi}{2},\\
E =& \alpha\left(\alpha-1\right)\omega^{\alpha-2}\cos\frac{\alpha\pi}{2},\\
F =& \alpha\left(\alpha-1\right)\omega^{\alpha-2}\sin\frac{\alpha\pi}{2},\\
O =& K_D\mu\omega^{\mu-1}\cos\frac{\mu\pi}{2} - \frac{\vartheta K_T}{\omega^{\vartheta+1}}\cos\frac{\vartheta\pi}{2} - \frac{\lambda K_I}{\omega^{\lambda+1}}\cos\frac{\lambda\pi}{2},\\
P =& K_D\mu\omega^{\mu-1}\sin\frac{\mu\pi}{2} + \frac{\vartheta K_T}{\omega^{\vartheta+1}}\sin\frac{\vartheta\pi}{2} + \frac{\lambda K_I}{\omega^{\lambda+1}}\sin\frac{\lambda\pi}{2},\\
Q =& K_D\mu\left(\mu-1\right)\omega^{\mu-2}\cos\frac{\mu\pi}{2}\\
&+ \frac{\vartheta\left(\vartheta+1\right)K_T}{\omega^{\vartheta+2}}\cos\frac{\vartheta\pi}{2} + \frac{\lambda\left(\lambda+1\right)K_I}{\omega^{\lambda+2}}\cos\frac{\lambda\pi}{2},
\end{aligned}$$

$$R = K_D\mu(\mu-1)\omega^{\mu-2}\sin\frac{\mu\pi}{2} - \frac{\vartheta(\vartheta+1)K_T}{\omega^{\vartheta+2}}\sin\frac{\vartheta\pi}{2} - \frac{\lambda(\lambda+1)K_I}{\omega^{\lambda+2}}\sin\frac{\lambda\pi}{2}.$$

4.2.1. The phase margin constraint

The phase margin specifications (4.1) can be interpreted in terms of the following relationship:

$$\begin{aligned} &Arg\left[G_P(j\omega_C)G_C(j\omega_C)\right] = -\pi + \phi_m, \\ &\Rightarrow \angle G_P(j\omega_C) + \angle G_C(j\omega_C) \\ &= -\pi + \phi_m \\ &\Rightarrow -\tan^{-1}\left(\frac{B}{A}\right) - \omega L + \tan^{-1}\left(\frac{N}{M}\right)\Big|_{\omega=\omega_C} \\ &= -\pi + \phi_m, \\ &\Rightarrow \tan^{-1}\left(\frac{B}{A}\right) - \tan^{-1}\left(\frac{N}{M}\right)\Big|_{\omega=\omega_C} \\ &= \pi - \phi_m - \omega L. \end{aligned} \tag{4.7}$$

4.2.2. The gain crossover frequency constraint

The gain crossover frequency specifications (4.2) narrates the following relationship:

$$\begin{aligned} |T(j\omega_C)| = \ &|G_P(j\omega_C)G_C(j\omega_C)| = 1, \\ &\Rightarrow \frac{K\sqrt{(M)^2+(N)^2}}{\sqrt{(A)^2+(B)^2}} - 1\Big|_{\omega=\omega_C} = 0. \end{aligned} \tag{4.8}$$

4.2.3. The robustness towards gain variations

The condition for the robustness of the system to the variations in gain (4.3) can be described as follows:

$$\frac{d}{d\omega}\left(Arg\left[G_P(j\omega)G_C(j\omega)\right]\right)\Big|_{\omega=\omega_c} = 0,$$

i.e.,

$$\frac{d}{d\omega}\left\{-\tan^{-1}\left(\frac{B}{A}\right) - \omega L + \tan^{-1}\left(\frac{N}{M}\right)\right\}\Big|_{\omega=\omega_C} = 0.$$

Now,

$$\frac{d}{d\omega}\left\{\tan^{-1}\left(\frac{B}{A}\right)\right\}\Big|_{\omega=\omega_C} = \frac{AD-BC}{A^2+B^2}\Big|_{\omega=\omega_C}.$$

Moreover,

$$\frac{d}{d\omega}\left\{\tan^{-1}\left(\frac{N}{M}\right)\right\}\Big|_{\omega=\omega_C} = \frac{(M)(P)-(N)(O)}{(M)^2+(N)^2}.$$

Therefore, the above constraint becomes the following:

$$\left(\frac{MP-NO}{M^2+N^2}\right) - \left(\frac{AD-BC}{A^2+B^2}\right) - L\Big|_{\omega=\omega_C} = 0. \tag{4.9}$$

4.2.4. The output disturbance rejection

The sensitivity function (4.4) for the output disturbance elimination provides the following expression:

$$\begin{aligned} &\left|\frac{1}{1+G_P(j\omega)G_C(j\omega)}\right|_{dB}\Big|_{\omega=\omega_s} = B_D dB, \\ &\Rightarrow \left|\frac{1}{1+G_P(j\omega)G_C(j\omega)}\right| \\ &= 10^{\frac{B_D}{20}}. \end{aligned}$$

Therefore,

$$|G_P(j\omega)G_C(j\omega)| = \frac{K\sqrt{M^2+N^2}}{\sqrt{A^2+B^2}}.$$

Hence, the above equation can be expressed as follows:

$$\frac{\sqrt{A^2+B^2}}{\sqrt{A^2+B^2}+K\sqrt{M^2+N^2}} - 10^{\frac{B_D}{20}} = 0\Big|_{\omega=\omega_s}. \tag{4.10}$$

4.2.5. The rejection of high-frequency noise

The complementary sensitivity function (4.5) meant for noise suppression produces the following relationship:

$$\begin{aligned} &\left|\frac{G_P(j\omega)G_C(j\omega)}{1+G_P(j\omega)G_C(j\omega)}\right|_{dB}\Big|_{\omega=\omega_t} = A_N dB \\ &\Rightarrow \left|\frac{G_P(j\omega)G_C(j\omega)}{1+G_P(j\omega)G_C(j\omega)}\right| \\ &= 10^{\frac{A_N}{20}}. \end{aligned}$$

Now, proceeding as per the previous section, we obtain the following:

$$\frac{K\sqrt{M^2+N^2}}{\sqrt{A^2+B^2}+K\sqrt{M^2+N^2}} - 10^{\frac{A_N}{20}} = 0\Big|_{\omega=\omega_t}. \tag{4.11}$$

4.2.6. The enhanced robustness towards gain variations

The constraint for the improved robustness of the system towards the system gain variation (4.6) can be expressed as follows:

$$\begin{aligned} &\frac{d}{d\omega}\left\{\frac{d}{d\omega}\left(Arg\left[G_P(j\omega)G_C(j\omega)\right]\right)\right\}\Big|_{\omega=\omega_c} = 0, \\ &\Rightarrow \frac{d}{d\omega}\left\{\left(\frac{MP-NO}{M^2+N^2}\right) - \left(\frac{AD-BC}{A^2+B^2}\right) - L\right\}\Big|_{\omega=\omega_c} = 0. \end{aligned}$$

Now,

$$\frac{d}{d\omega}\left(\frac{MP-NO}{M^2+N^2}\right)\Big|_{\omega=\omega_c} = \frac{\left(M^2+N^2\right)(MR-NQ)-2\,(MP-NO)\,(MO+NP)}{\left(M^2+N^2\right)^2}.$$

Moreover,

$$\frac{d}{d\omega}\left(\frac{AD-BC}{A^2+B^2}\right)\Big|_{\omega=\omega_c} = \frac{\left(A^2+B^2\right)(AF-BE)-2\,(AD-BC)\,(AC+BD)}{\left(A^2+B^2\right)^2}.$$

Additionaly,

$$\frac{d}{d\omega}\,(L)|_{\omega=\omega_c} = 0.$$

Therefore, for $\omega = \omega_C$, we get the following:

$$\frac{\left(M^2+N^2\right)(MR-NQ)-2\,(MP-NO)\,(MO+NP)}{\left(M^2+N^2\right)^2} - \frac{\left(A^2+B^2\right)(AF-BE)-2\,(AD-BC)\,(AC+BD)}{\left(A^2+B^2\right)^2} = 0. \tag{4.12}$$

Now, considering any of the above equations as the objective function and the other five equations as the nonlinear constraints, the MATLAB optimization toolbox fmincon() with the interior-point algorithm can be used to minimize this above constraint optimization problem and determine the appropriate values of the FOTID parameters.

4.3. The fmincon() function

The fmincon() is used to determine the constraint minimal value of any function that consists of several variables. It evaluates the problem in the following process:

$$\underset{X}{minimize}\ F(X),$$

subject to:

$$Linear: \begin{cases} \mathrm{A} * X \leqslant B\ (inequality\ constraint), \\ \mathrm{A}_{eq} * X = B_{eq}\ (equality\ constraint). \end{cases}$$

$$Nonlinear: \begin{cases} \mathrm{C}(X) \leqslant 0\ (inequality\ constraint), \\ \mathrm{C}_{eq}(X) = 0\ (equality\ constraint). \end{cases}$$

$$Limit: \Big\{ \mathrm{L}B \leqslant X \leqslant UB\ (lower\ and\ upper\ bound).$$

For the above minimization problem, the function variable is as follows:

$$X = [K_T, K_I, K_D, \lambda, \mu, n],$$

which holds the parameter of the controller. Furthermore, for the successful evaluation of the solution by the fmincon(), prior knowledge of the initial set of value

$$X(0) = [K_T(0), K_I(0), K_D(0), \lambda(0), \mu(0), n(0)]$$

is desired. Either some random initial values or the results obtained from any optimization algorithm can be used as the initial set of guess values.

The fmincon() uses four basic algorithms for the evaluation of the desired solution: interior point, sequential programming, active set, and the trust region reflective. The interior point algorithm can efficiently manage both sparse (large) and dense (small) problems [46]. It usually satisfies its boundary limits for all iterations and can easily recover from problems such as results being (*NAN*) or infinite values.

In this article, Eq (4.9) is considered as the objective function $F(X)$ to be minimized. The Eqs (4.7), (4.8), and (4.10)–(4.12) are the nonlinear equality constraint $C_{eq}(X)$ and other parameters such as $A, B, A_{eq}, B_{eq}, C(X)$ are zero. Furthermore, instead of an arbitrary initial guess, this article considers the values obtained from the time domain-based procedure as the initial value.

The process includes the minimization of error-based objective functions, as the nullification of error can provide a desirable closed-loop system performance. The PSO algorithm with the ITAE objective function is used in this article for this purpose.

5. Numerical examples

The FOTID tuning strategy proposed in the previous section is implemented by citing suitable examples as discussed below. As the above procedure is meant both for integer and non-integer order systems, this article explores both integer and fractional order systems and designs suitable FOTID controllers for them.

5.1. Example 1

Consider a fractional order interval process that has a transfer function as [47]:

$$G_P(s) = \frac{\left[K', \bar{K}'\right]}{[\tau, \bar{\tau}]\, s^{[\gamma, \bar{\gamma}]} + 1} \Rightarrow G_{P1}(s) = \frac{1}{2s^{1.4} + 1}.$$

Here, let $K' = 1$, $\tau = 2$, and the nominal order of the plant be $\gamma = 1.4$. However, the variation in the system order can be within the following:

$$[\gamma, \bar{\gamma}] = [1.0, 1.8]\,.$$

Now, by converting the above system from the time-constant form to the pole-zero form, we obtain the following:

$$G_{P1}(s) = \frac{0.5}{s^{1.4} + 0.5}.$$

Therefore, as per Eq (2.1), we have the parameters K=0.5, a=0.5, α=1.4, and L=0, sec. Now, using the Oustaloup filter approximation of the 5th order while considering a frequency range of $\left(10^{-3}, 10^{3}\right)$ rad/seconds, the step response of the above system is shown in Figure 3 and the relevant information is mentioned in Table 1. Although it indicates a minimal settling time of $t_s = 6.0250$ seconds, it has a steady state error $e_{ss} = 0.4985$.

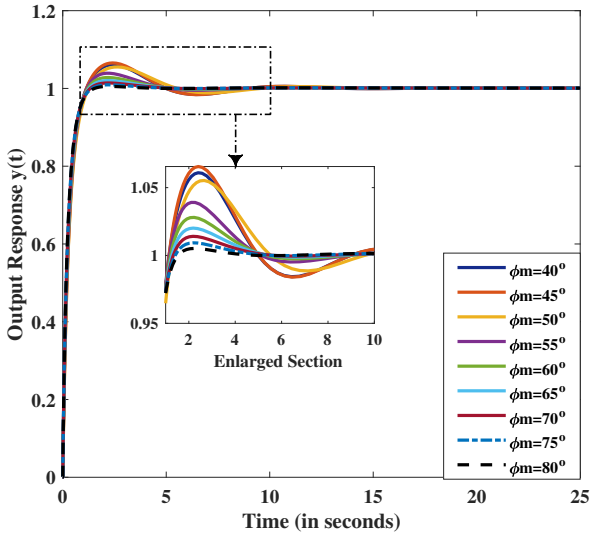

Figure 3. The step responses of the system for different phase margins.

Table 1. Time domain specifications.

System	Rise time (t_r in seconds)	Settling time (t_s in seconds)	Peak overshoot (M_p)	Steady state error (e_{ss})
Original system	1.2750	6.0250	0	-0.4985
FOPID-1 [47]	1.8362	14.2541	15.6974	0.0046
FOPID-2 [47]	2.0629	11.0888	11.6251	0.0049
FOTID (proposed)	0.5476	1.0262	0.4620	0.0006

This brings the need of designing a suitable controller for the performance improvement of the corresponding system. The parameter evaluation of the FOTID using the above procedure is described as follows.

In tis article, as the above-proposed optimization problems (4.7)–(4.12) are nonconvex, their corresponding analytical evaluations are difficult. The MATLAB nonlinear optimization toolbox fmincon() can be used to perform the above minimization and produce optimal results. The FOTID parameters that correspond to different phase margins presented in Table 2.

Table 2. FOTID parameters correspond to various phase margins.

Phase margin	K_T	K_I	K_D	λ	μ	n	Objective function
ϕ_m=40°	0.1	5.3669	6.9375	1.0823	0.4402	3	0.87743
ϕ_m=45°	1.6561	4.2453	6.3705	1.1000	0.4904	3	0.52033
ϕ_m=50°	1.8617	4.0214	6.6709	1.1000	0.4957	3	0.43153
ϕ_m=55°	2.0207	3.8544	6.9028	1.1000	0.4995	3	0.34695
ϕ_m=60°	2.1460	3.7265	7.0842	1.1000	0.5024	3	0.27545
ϕ_m=65°	2.2261	3.6316	7.2314	1.1000	0.5042	3	0.22150
ϕ_m=70°	2.2888	3.5554	7.3525	1.1000	0.5056	3	0.17707
ϕ_m=75°	2.3392	3.4929	7.4538	1.1000	0.5064	3	0.14009
ϕ_m=80°	2.3806	3.4407	7.5397	1.1000	0.5076	3	0.10893

Let the search region of the solution be

$$K_T, K_I, K_D \in (0.1, 10),\ \lambda,\ \mu \in (0.1, 1.1),\ \ n \in (2, 3),$$

and the initial guess be

$$K_T(0) = 2.0549,\ \ K_I(0) = 4.1878,\ \ K_D(0) = 8.9832,$$
$$\lambda(0) = 1.0542,\ \ \ \mu(0) = 0.5065,\ \ \ n(0) = 2.9197.$$

Furthermore, the gain cross-over frequency $\omega_C = 0.8$ rad/s, the phase margin $\phi_m \in (40^o, 80^o)$, the noise attenuation $A_N = -100$ dB for $\omega \geq \omega_t = 100$ rad/s, and the value of the sensitivity function $B_D = -100$ dB for $\omega \leq \omega_S = 0.001$ rad/s.

Now, considering Eq (4.9) as the objective function, and Eqs (4.7), (4.8), and (4.10)–(4.12) as the nonlinear constraints, the fmincon() produces the controller parameters as mentioned in Table 2. It is evident that the objective function is minimum for $\phi_m = 80^o$, thus producing superior time response performances as seen in Figure 4.

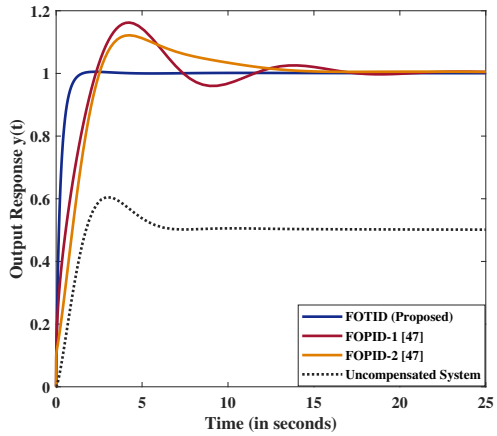

Figure 4. The step responses of the system with different fractional order controllers.

The Bode diagram for the above process with different integral and non-integral order controllers is presented in Figure 5.

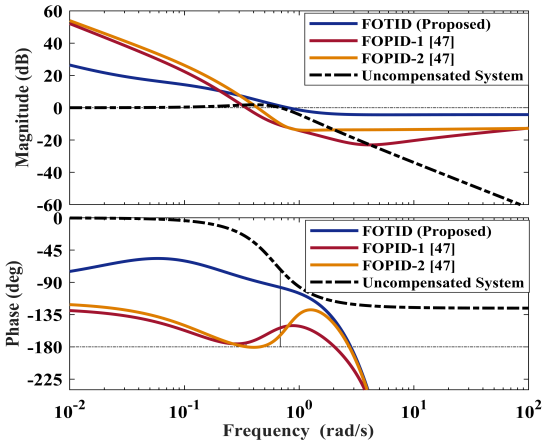

Figure 5. The Bode plot of the system with various non-integer order controllers.

It reveals that the system with FOTID controller achieves the desired value of the phase margin, i.e., $\phi_m = 80^o$ and the phase angle response remains almost flat about the gain cross over frequency $\omega_C = 0.8$ rad/s.

Thus, the desired FOTID controller thus obtained from the above procedure is expressed as follows:

$$G_{C1-FOTID}(s) = \frac{2.3806}{s^{0.3333}} + \frac{3.4407}{s^{1.1000}} + 7.5397\, s^{0.5076}.$$

The behavior of the system with different controllers under variations in the system parameters is mentioned in Table 3 and the responses are shown in Figure 6.

Table 3. Time domain specification of systems corresponds to parameter variations.

Systems	Parameter variations	t_r (in seconds)	t_s (in seconds)	M_p	e_{ss}
FOPID-1 [47]	$\gamma = 1.2$	2.1544	16.1735	17.6254	0.0031
	$\gamma = 1.6$	1.4933	12.7639	15.8990	0.0016
	$K = 2$	1.1911	8.6366	10.5581	0.0011
	$K = 3$	0.9077	5.0482	7.7288	0.0007
	$\tau = 1.0$ s	1.9734	8.4062	7.2927	0.0029
	$\tau = 3.0$ s	2.0687	22.7707	24.7498	0.0294
FOPID-2 [47]	$\gamma = 1.2$	2.4710	10.9142	14.1676	0.0067
	$\gamma = 1.6$	1.6830	12.2491	17.0186	0.0048
	$K = 2$	1.2909	7.8685	11.2665	0.0024
	$K = 3$	1.0021	4.1155	10.6553	0.0016
	$\tau = 1.0$ s	2.0988	12.9036	7.4529	0.0047
	$\tau = 3.0$ s	2.2173	17.9112	25.5713	0.0022
FOTID (Proposed)	$\gamma = 1.2$	0.8142	1.9110	1.8091	0.0006
	$\gamma = 1.6$	0.4545	1.8560	6.6025	0.0007
	$K = 2$	0.2699	0.5694	0.2485	0.0003
	$K = 3$	0.1754	0.3985	0.1675	0.0002
	$\tau = 1.0$ s	0.3079	3.3084	0.6129	0.0007
	$\tau = 3.0$ s	0.7289	4.2040	4.9510	0.0004

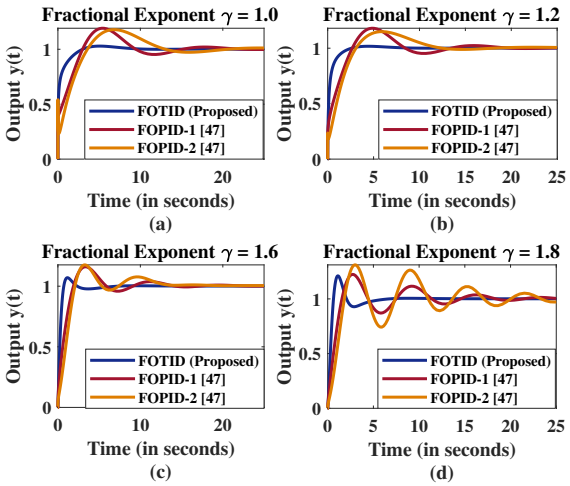

Figure 6. The step response comparison between controllers under parameter variation.

Here, the fractional exponent γ is varied over (1.0–1.6), the system gain K is varied over (1.0–3.0), the time constant τ is varied over the range (1.0 s−3.0 s), and the effectiveness of the controllers to address the changes to system dynamics are observed. The superiority of the FOTID controller over FOPID is noticed in the above responses.

5.2. *Example 2*

Consider a first-order interval plant with a delay time as follows [48]:

$$G_P(s) = \frac{\left[K', \bar{K'}\right]}{[\tau, \bar{\tau}]\, s + 1} e^{-[L,\bar{L}]s}.$$

Here, the values of the interval variables are:

$$\left[K', \bar{K'}\right] = [2, 4], \quad [\tau, \bar{\tau}] = [60, 80] \text{ seconds},$$

and

$$\left[L, \bar{L}\right] = [0.5, 1] \text{ seconds}.$$

Hence, considering the values

$$K = 4, \quad \tau = 60 \text{ seconds},$$

and $L = 1$ second, the above integral first-order transfer function is presented as follows:

$$G_{P2}(s) = \frac{K'}{\tau s + 1} e^{-Ls} = \frac{4}{60s + 1} e^{-1s}.$$

Likewise, converting the above transfer function from the time constant form to the pole-zero form leads to the following:

$$G_{P2}(s) = \frac{0.0667}{s + 0.0167} e^{-1s}.$$

Now, concerning Eq (2.1), the process parameters are

$$K = 0.0667, \quad a = 0.0167, \quad \alpha = 1.0,$$

and $L = 1.0$ s. The step response of the above system is presented in Figure 7 and the corresponding information is provided in Table 4.

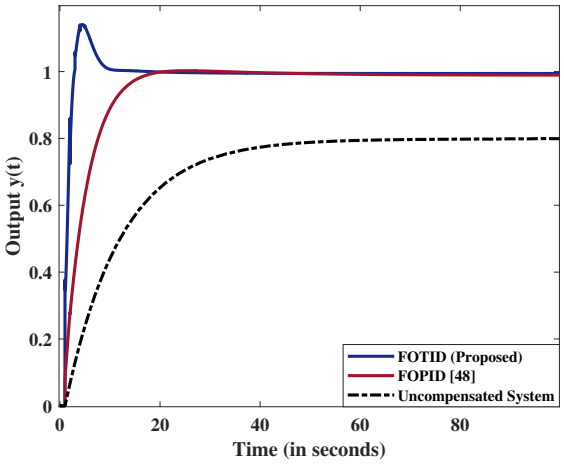

Figure 7. The step response comparison within different controllers.

Table 4. Time domain specifications.

Systems	t_r (in seconds)	t_s (in seconds)	M_p	e_{ss}
Original system	24.5400	45.4712	—	-0.2008
FOPID [48]	8.9719	14.6167	1.2354	-0.0094
FOTID (Proposed)	1.2118	8.0963	17.1882	-0.0055

It can be observed from the step response of the uncompensated system that, it has a rise time of $t_R = 24.54$ seconds, a settling time of $t_s = 45.4712$ seconds, and a steady state error of $e_{ss} = 0.2008$. This indicates the requirement of a suitable controller for the improvement of the transient and steady-state performances of the above system. The parameter debugging of the FOTID controller using the above loop shaping method is presented below.

Consider the desired solution to be within

$$K_T, K_I, K_D \in (0.1, 10), \quad \lambda, \mu \in (0.1, 1.5), \quad \text{and} \quad n \in (2, 3),$$

and the initial guess be

$$K_T(0) = 1.9325, \quad K_I(0) = 9.8778, \quad K_D(0) = 8.9152,$$
$$\lambda(0) = 0.13896, \quad \mu(0) = 0.98984, \quad n(0) = 2.6853.$$

Let the parameters $\omega_C = 0.16$ rad/s, $\phi_m \in (40^o, 60^o)$, $A_N = -100$ dB for $\omega \geq \omega_t = 100$ rad/s, $B_D = -100$ dB for $\omega \leq \omega_S = 0.001$ rad/s. Now, with Eq (4.9) as the objective and the problems (4.7), (4.8), (4.10)–(4.12) as the nonlinear constraints, the fmincon() produces the results as given in Table 5.

Table 5. FOTID parameters correspond to various phase margins.

Phase margin	K_T	K_I	K_D	λ	μ	n	Objective function
ϕ_m=40°	1.6049	8.7985	2.0655	0.1000	1.1278	2	-1.1885
ϕ_m=45°	1.5804	8.8589	3.0468	0.1000	1.0913	2	-1.1100
ϕ_m=50°	1.5600	8.8982	3.9948	0.1000	1.0622	2	-1.0272
ϕ_m=55°	1.5430	8.9211	4.9239	0.1000	1.0360	2	-0.9395
ϕ_m=60°	1.5300	8.9237	5.8462	0.1000	1.0109	2	-0.8460

The comparison of the responses for different phase margins is presented in Figure 8, thus indicating a superior transient performance for

$$\phi_m = 50^o.$$

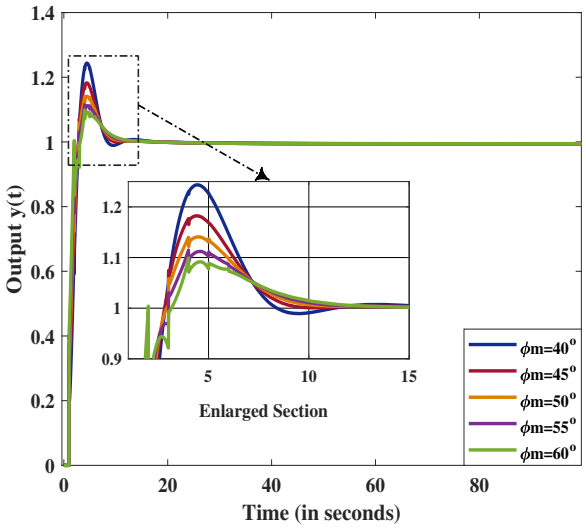

Figure 8. The step response of the system for different phase margins.

The time response comparison of the above system under the influence of different controllers is presented in Figure 7. Although both FOTID and FOPID nullifies the steady state error, a minimal rise and setting time are observed in the case of FOTID controller. Likewise, the Bode diagram for the above process is provided in Figure 9. The desired phase margin

$$\phi_m = 50^o$$

at

$$\omega_C = 0.16 \text{ rad/seconds}$$

is obtained by using the FOTID controller.

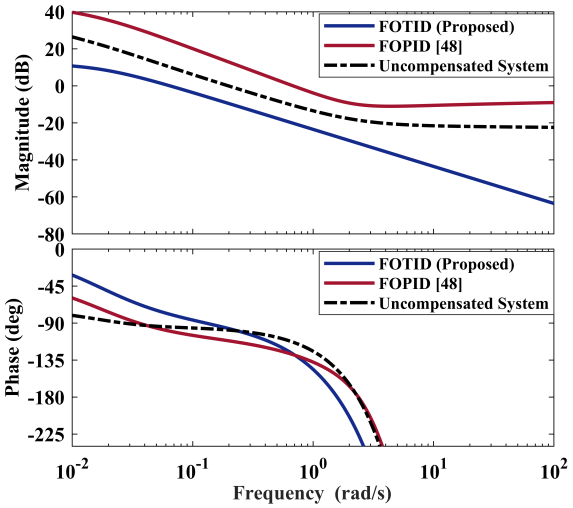

Figure 9. The Bode plot of the system with different fractional controllers.

Now, the desired value of the FOTID controller is presented as follows:

$$G_{C2-FOTID}(s) = \frac{1.5600}{s^{0.5000}} + \frac{8.8982}{s^{0.1000}} + 3.9948s^{1.0622}.$$

Similarly, the performance of the system having different controllers in the presence of variations in the system parameters such as the gain, time constant, and time delay, etc. is provided in Table 6.

Table 6. Time domain specification of systems corresponds to parameter variations.

Systems	Parameter variations	t_r (in seconds)	t_s (in seconds)	M_p	e_{ss}
FOPID [48]	K = 2.0	18.1018	28.4793	1.0100	-0.0202
	K = 3.0	12.0735	19.2427	1.2641	-0.0138
	T = 70 s	10.3267	16.2065	1.9196	-0.0083
	T = 80 s	11.6807	40.0524	2.4196	-0.0061
	L = 0.5 s	10.0398	15.7636	1.1651	-0.0104
	L = 0.75 s	9.4901	15.1441	1.2257	-0.0104
FOTID (Proposed)	K = 2.0	3.1483	15.3746	10.3348	-0.0110
	K = 3.0	1.9231	10.7370	13.3723	-0.0073
	T = 70 s	1.5469	9.5507	14.9772	-0.0053
	T = 80 s	1.9130	11.0570	13.9177	-0.0051
	L = 0.5 s	2.0078	10.0670	7.3174	-0.0055
	L = 0.75 s	1.5878	9.2624	10.4385	-0.0055

For the above interval system, the parameters are varied over

$$\left[K', \bar{K}'\right] = [2, 4], \quad [\tau, \bar{\tau}] = [60, 80] \text{ seconds},$$

and

$$\left[L, \bar{L}\right] = [0.5, 1] \text{ seconds.}$$

The efficiency of the controllers to nullify the effect of the above changes in the system dynamics is observed in Figure 10. The supremacy of the FOTID controller over FOPID is observed from the above step responses.

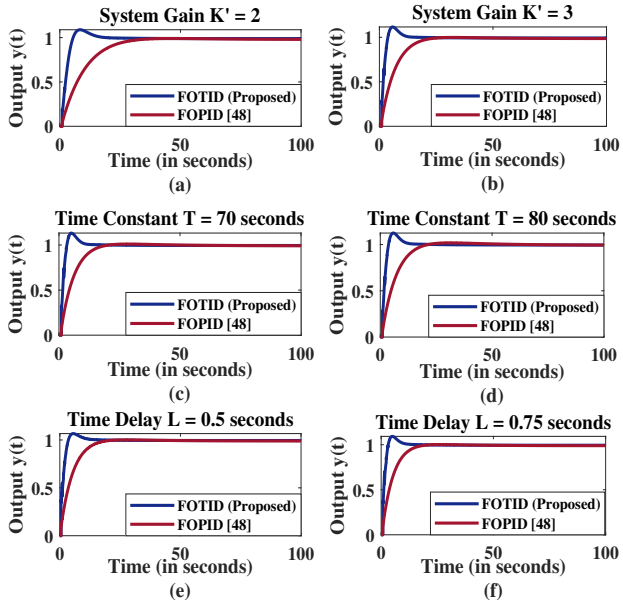

Figure 10. The step response comparison within controllers under parameter variation.

6. Conclusions

In this paper, the loop shaping-based parameter estimation of the FOTID controller was presented. A non-integral order process under the influence of time delay was examined to implement the above-proposed control strategy. As the analytical solution process of a system with a FOTID controller needs six simultaneous equations, this paper added an enhanced robustness to gain variations (more flat phase)in the condition as the sixth constraint to the existing loop shaping parameter tuning method of the FOPID controller.

The nonlinear optimization toolbox fmincon() was utilized to minimize the objective functions under constraints and to obtain the desired system performance. In this article, the robustness to gain variation condition was considered as the minimization function, and the remaining were nonlinear equality constraints. As the success of the fmincon() precisely depends upon the initial guess values, this article considered the results obtained from the PSO as the initial guess.

The effectiveness of the proposed deterministic procedure was justified through numerical simulations that considered different integral and fractional interval models. The comparison between the FOTID and FOPID signifies the supremacy of FOTID in terms of the minimal rise time, the minimal settling time, and diminished error at a steady state. Additionally, the robustness of the proposed controller that corresponded to the system parameter variations was examined. It was observed that the FOTID controller tuned by this proposed method not only showed better system performances, but also exhibited significant disturbance rejection characteristics.

The above work can be extended and the effectiveness of FOTID can be verified by changing the objective functions and constraints. Furthermore, as the number of equations sufficiently increase; therefore, instead of a single objective, a multi-objective parameter estimation procedure can also be explored.

Conflict of interest

The authors declare that they have no conflicts of interest for this research.

References

1. P. Cominos, N. Munro, PID controllers: recent tuning methods and design to specification, *IEE Proc. Control Theory Appl.*, **149** (2002), 46–53. https://doi.org/10.1049/ip-cta:20020103

2. O. Defterli, D. Baleanu, A. Jajarmi, S. S. Sajjadi, N. Alshaikh, J. Asad, Fractional treatment: an accelerated mass-spring system, *Rom. Reports Phys.*, **74** (2022), 122.

3. D. Baleanu, S. Arshad, A. Jajarmi, W. Shokat, F. A. Ghassabzade, M. Wali, Dynamical behaviours and stability analysis of a generalized fractional model with a real case study, *J. Adv. Res.*, **48** (2023), 157–173. https://doi.org/10.1016/j.jare.2022.08.010

4. D. Baleanu, M. Hasanabadi, A. M. Vaziri, A. Jajarmi, A new intervention strategy for an HIV/AIDS transmission by a general fractional modeling and an optimal control approach, *Chaos Solitons Fract.*, **167** (2023), 113078. https://doi.org/10.1016/j.chaos.2022.113078
5. D. Xue, T. Li, L. Liu, A MATLAB toolbox for multivariable linear fractional-order control systems, *2017 29th Chinese Control and Decision Conference (CCDC)*, 2017, 1894–1899. https://doi.org/10.1109/CCDC.2017.7978826
6. A. Tepljakov, E. Petlenkov, J. Belikov, FOMCOM: a MATLAB toolbox for fractional-order system identification and control, *Int. J. Microelectron. Comput. Sci.*, **2** (2011), 51–62.
7. I. Podlubny, Fractional-order systems and $PI^{\lambda}D^{\mu}$ controllers, *IEEE Trans. Autom. Control*, **44** (1999), 208–214. https://doi.org/10.1109/9.739144
8. C. A. Monje, B. M. Vinagre, V. Feliu, Y. Chen, Tuning and auto-tuning of fractional order controllers for industry applications, *Control Eng. Practice*, **16** (2008), 798–812. https://doi.org/10.1016/j.conengprac.2007.08.006
9. I. Petráš, *Fractional-order nonlinear systems: modeling, analysis, and simulation*, Springer Science & Business Media, 2011. https://doi.org/10.1007/978-3-642-18101-6
10. B. Lurie, *Three-parameter tunable tilt-Integral-derivative (TID) controller*, Patent Number US 5278209, 1994.
11. S. K. Bhagat, N. R. Babu, L. C. Saikia, T. Chiranjeevi, R. Devarapalli, F. P. G. Márquez, A review on various secondary controllers and optimization techniques in automatic generation control, *Arch. Comput. Methods Eng.*, **30** (2023), 3081–3111. https://doi.org/10.1007/s11831-023-09895-z
12. K. Gnaneshwar, P. K. Padhy, Robust design of tilted integral derivative controller for non-integer order processes with time delay, *IETE J. Res.*, **69** (2023), 6198–6209. https://doi.org/10.1080/03772063.2021.2004462
13. C. Lu, R. Tang, Y. Chen, C. Li, Robust tilt-integral-derivative controller synthesis for first-order plus time delay and higher-order systems, *Int. J. Robust Nonlinear Control*, **33** (2023), 1566–1592. https://doi.org/10.1002/rnc.6449
14. M. Z. Malik, S. Zhang, G. Chen, M. L. Alghaythi, Robust tilt-integral-derivative controllers for fractional-order interval systems, *Mathematics*, **11** (2023), 2763. https://doi.org/10.3390/math11122763
15. F. Merrikh-Bayat, A uniform LMI formulation for tuning PID, multi-term fractional-order PID, and tilt-integral-derivative (TID) for integer and fractional-order processes, *ISA Trans.*, **68** (2017), 99–108. https://doi.org/10.1016/j.isatra.2017.03.002
16. D. Guha, P. K. Roy, S. Banerjee, Equilibrium optimizer-tuned cascade fractional-order 3DOF-PID controller in load frequency control of power system having renewable energy resource integrated, *Int. Trans. Electr. Energy Syst.*, **31** (2021), e12702. https://doi.org/10.1002/2050-7038.12702
17. P. N. Topno, S. Chanana, Load frequency control of a two-area multi-source power system using a tilt integral derivative controller, *J. Vib. Control*, **24** (2018), 110–125. https://doi.org/10.1177/1077546316634562
18. M. Ali, H. Kotb, M. K. AboRas, H. N. Abbasy, Frequency regulation of hybrid multi-area power system using wild horse optimizer based new combined fuzzy fractional-order PI and TID controllers, *Alex. Eng. J.*, **61** (2022), 12187–12210. https://doi.org/10.1016/j.aej.2022.06.008
19. M. Ranjan, R. Shankar, A novel arithmetic optimization algorithm-based 2DOF tilted-integral-derivative controller for restructured LFC, In: K. Namrata, N. Priyadarshi, R. C. Bansal, J. Kumar, *Smart energy and advancement in power technologies*, Springer, 2022, 513–525. https://doi.org/10.1007/978-981-19-4975-3_41
20. M. A. El-Dabah, S. Kamel, M. A. Y. Abido, B. Khan, Optimal tuning of fractional-order proportional, integral, derivative, and tilt-integral-derivative based power system stabilizers using Runge Kutta optimizer, *Eng. Reports*, **4** (2022), e12492. https://doi.org/10.1002/eng2.12492

21. P. N. Topno, S. Chanana, Differential evolution algorithm-based tilt integral derivative control for LFC problem of an interconnected hydro-thermal power system, *J. Vib. Control*, **24** (2018), 3952–3973. https://doi.org/10.1177/1077546317717866

22. R. K. Sahu, S. Panda, A. Biswal, G. C. Sekhar, Design and analysis of tilt integral derivative controller with filter for load frequency control of multi-area interconnected power systems, *ISA Trans.*, **61** (2016), 251–264. https://doi.org/10.1016/j.isatra.2015.12.001

23. J. M. R. Chintu, R. K. Sahu, S. Panda, Design and analysis of two degree of freedom tilt integral derivative controller with filter for frequency control and real time validation, *J. Electr. Eng.*, **71** (2020), 388–396. https://doi.org/10.2478/jee-2020-0053

24. R. K. Khadanga, S. Padhy, S. Panda, A. Kumar, Design and analysis of tilt integral derivative controller for frequency control in an islanded microgrid: a novel hybrid dragonfly and pattern search algorithm approach, *Arabian J. Sci. Eng.*, **43** (2018), 3103–3114. https://doi.org/10.1007/s13369-018-3151-0

25. K. Singh, M. Amir, F. Ahmad, M. A. Khan, An integral tilt derivative control strategy for frequency control in multi microgrid system, *IEEE Syst. J.*, **15** (2020), 1477–1488. https://doi.org/10.1109/JSYST.2020.2991634

26. S. K. Bhagat, L. C. Saikia, N. R. Babu, Application of artificial hummingbird algorithm in a renewable energy source integrated multi-area power system considering fuzzy based tilt integral derivative controller, *e-Prime Adv. Electr. Eng. Electron. Energy*, **4** (2023), 100153. https://doi.org/10.1016/j.prime.2023.100153

27. A. Rai, D. K. Das, The development of a fuzzy tilt integral derivative controller based on the sailfish optimizer to solve load frequency control in a microgrid, incorporating energy storage systems, *J. Energy Storage*, **48** (2022), 103887. https://doi.org/10.1016/j.est.2021.103887

28. S. Patel, B. Mohanty, H. M. Hasanien, Competition over resources optimized fuzzy TIDF controller for frequency stabilization of the hybrid micro-grid system, *Int. Trans. Electr. Energy Syst.*, **30** (2020), e12513. https://doi.org/10.1002/2050-7038.12513

29. E. Isen, Determination of different types of controller parameters using metaheuristic optimization algorithms for buck converter systems, *IEEE Access*, **10** (2022), 127984–127995. https://doi.org/10.1109/ACCESS.2022.3227347

30. T. Amieur, M. Bechouat, M. Sedraoui, M. Kahla, H. Guessoum, A new robust tilt-PID controller based upon an automatic selection of adjustable fractional weights for permanent magnet synchronous motor drive control, *Electr. Eng.*, **103** (2021), 1881–1898. https://doi.org/10.1007/s00202-020-01192-3

31. T. Chiranjeevi, N. R. Babu, S. K. Pandey, R. K. Patel, U. K. Gupta, R. I. Vais, et al., Maiden application of flower pollination algorithm-based tilt integral derivative controller with filter for control of electric machines, *Mater. Today*, **47** (2021), 2541–2546. https://doi.org/10.1016/j.matpr.2021.05.049

32. S. K. Bhagat, L. C. Saikia, N. R. Babu, Application of an optimal tilt controller in a partial loading schedule of multi-area power system considering HVDC link and virtual inertia, *ISA Trans.*, **146** (2023), 437–450. https://doi.org/10.1016/j.isatra.2023.12.018

33. M. Aidoud, V. Feliu-Batlle, A. Sebbagh, M. Sedraoui, Small signal model designing and robust decentralized tilt integral derivative TID controller synthesizing for twin rotor MIMO system, *Int. J. Dyn. Control*, **10** (2022), 1657–1673. https://doi.org/10.1007/s40435-022-00916-6

34. S. Priyadarshani, K. R. Subhashini, J. K. Satapathy, Pathfinder algorithm optimized fractional order tilt-integral-derivative (FOTID) controller for automatic generation control of multi-source power system, *Microsyst. Technol.*, **27** (2021), 23–35. https://doi.org/10.1007/s00542-020-04897-4

35. M. Sharma, S. Prakash, S. Saxena, S. Dhundhara, Optimal fractional-order tilted-integral-derivative controller for frequency stabilization in hybrid power system using salp swarm algorithm, *Electr. Power Compon. Syst.*, **48** (2020), 1912–1931. https://doi.org/10.1080/15325008.2021.1906792

36. D. Guha, P. K. Roy, S. Banerjee, Disturbance observer-aided optimized fractional-order three-degree-of-freedom tilt-integral-derivative controller for load frequency control of power systems, *IET Gene. Transm. Distrib.*, **15** (2021), 716–736. https://doi.org/10.1049/gtd2.12054

37. A. K. Patra, D. Rath, Design of PV system based on 3-degree of freedom fractional order tilt-integral-derivative controller with filter, *J. Inst. Eng. India*, **103** (2022), 1533–1548. https://doi.org/10.1007/s40031-022-00739-1

38. S. Mohapatra, D. Choudhury, K. Bishi, S. Keshari, B. K. Dakua, C. Kaunda, A comparison between the FOTID and FOPID controller for the close-loop speed control of a DC motor system, *2023 International Conference on Artificial Intelligence and Applications (ICAIA) Alliance Technology Conference (ATCON-1)*, 2023. https://doi.org/10.1109/ICAIA57370.2023.10169248

39. E. A. Mohamed, M. Aly, M. Watanabe, New tilt fractional-order integral derivative with fractional filter (TFOIDFF) controller with artificial hummingbird optimizer for LFC in renewable energy power grids, *Mathematics*, **10** (2022), 3006. https://doi.org/10.3390/math10163006

40. M. Sharma, S. Prakash, S. Saxena, Robust load frequency control using fractional-order TID-PD approach via salp swarm algorithm, *IETE J. Res.*, **69** (2023), 2710–2726. https://doi.org/10.1080/03772063.2021.1905084

41. H. Patel, V. Shah, An optimized intelligent fuzzy fractional order TID controller for uncertain level control process with actuator and system component uncertainty, In: B. Bede, M. Ceberio, M. De Cock, V. Kreinovich, *Fuzzy information processing 2020*, Springer International Publishing, 2021, 183–195. https://doi.org/10.1007/978-3-030-81561-5_16

42. A. K. Naik, N. K. Jena, S. Sahoo, B. K. Sahu, Optimal design of fractional order tilt-integral derivative controller for automatic generation of power system integrated with photovoltaic system, *Electrica*, **24** (2024), 140–153. https://doi.org/10.5152/electrica.2024.23044

43. A. Ranjan, U. Mehta, Fractional-order tilt integral derivative controller design using IMC scheme for unstable time-delay processes, *J. Control Autom. Electr. Syst.*, **34** (2023), 907–925. https://doi.org/10.1007/s40313-023-01020-6

44. S. Kumari, G. Shankar, Maiden application of cascade tilt-integral-tilt-derivative controller for performance analysis of load frequency control of interconnected multi-source power system, *IET Gene. Transm. Distrib.*, **13** (2019), 5326–5338. https://doi.org/10.1049/iet-gtd.2018.6726

45. C. M. Ionescu, E. H. Dulf, M. Ghita, C. I. Muresan, Robust controller design: recent emerging concepts for control of mechatronic systems, *J. Franklin Inst.*, **357** (2020), 7818–7844. https://doi.org/10.1016/j.jfranklin.2020.05.046

46. Z. Wu, J. Viola, Y. Luo, Y. Chen, D. Li, Robust fractional-order [proportional integral derivative] controller design with specification constraints: more flat phase idea, *Int. J. Control*, **97** (2021), 111–129. https://doi.org/10.1080/00207179.2021.1992498

47. X. Li, L. Gao, Robust fractional-order PID tuning method for a plant with an uncertain parameter, *Int. J. Control Autom. Syst.*, **19** (2021), 1302–1310. https://doi.org/10.1007/s12555-019-0866-y

48. C. Yeroglu, N. Tan, Note on fractional-order proportional-integral-differential controller design, *IET Control Theory Appl.*, **5** (2011), 1978–1989. https://doi.org/10.1049/iet-cta.2010.0746

AIMS Press